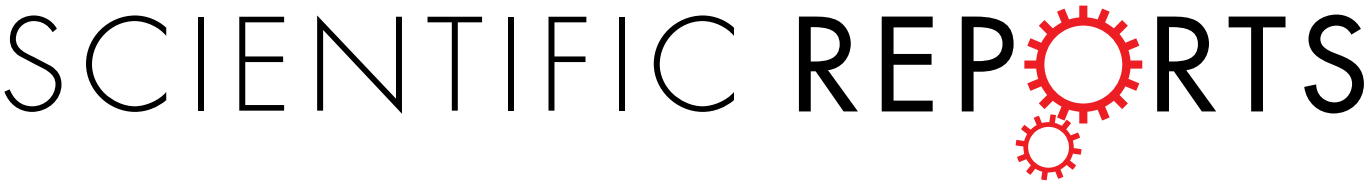

OPEN

Synthesis and Characterization of Porous $MnCo_2O_4$ for Electrochemical Determination of Cadmium ions in Water Samples

Received: 24 November 2016
Accepted: 9 March 2017
Published online: 05 April 2017

Murugan Velmurugan & Shen-Ming Chen

To utilize the maximum activity of nanomaterials, it was specifically synthesized by appropriate physicochemical properties. In that aspect, we have described the synthesis of porous $MnCo_2O_4$ by simple chemical route and applied for the selective detection of cadmium (Cd (II)). The as-prepared porous $MnCo_2O_4$ was characterized by scanning electron microscopy (SEM), transmission electron microscopy (TEM), Brunauer–Emmett–Teller (BET) adsorption isotherm, X-ray diffraction pattern analysis (XRD), Fourier transform infra-red spectroscopy (FT-IR), energy dispersive X-ray (EDX) and electrochemical techniques. The porous $MnCo_2O_4$ exhibited an excellent electrochemical behaviour and good analytical response towards the determination of Cd (II). Those analytical factors such as pH, deposition potential and deposition time are optimized by using differential pulse anodic stripping voltammetry (DPASV). A wide linear concentration range from 2.3 to 120 µg L^{-1}, limit of detection (LOD) of 0.72 µg L^{-1} and the limit of quantification (LOQ) of 0.91 µg L^{-1} were achieved for determination of Cd (II). The selectivity of the developed sensor was explored in the presence of co-interfering ions. Also our sensor exhibits a good stability, reproducibility and repeatability. In addition, the practicability of proposed sensor was evaluated for the detection of Cd (II) in real water samples.

Discharge of toxic heavy metal ions to the environment causes most harmful issues to the human and ecosystem. For occasion, the industry of ceramic, semiconductors, pharmaceutical, metallurgical, agricultural and petrochemicals contaminates the surrounding water and soil[1–3]. The Cd is one of the toxic heavy metal, which causes nephrotoxicity, flu-like symptoms, renal tubular dysfunction, bone demineralization and cancers even for the intake of trace level through contaminated food and water[4–8]. Therefore, the international agency of research of cancer (IARC) classified the cadmium as a carcinogenic substance[9]. Moreover, the world health organization (WHO) and United States Environmental Production Agency (EPA) have defined the maximum level of Cd in drinking water as 0.003–0.005 µg L^{-1} [10,11]. Therefore, the detection of Cd is essential in water treatment and soil analysis. There are several methods such as inductively coupled plasma mass spectrometry[12,13], inductively coupled plasma atomic emission spectrometry[14], atomic absorption spectrometry[15], atomic fluorescence spectrometry[16] and UV–Visible spectroscopy[17]. All the aforementioned methods offer good precision and high resolution, however, they are more expensive and needs trained technicians to handle the instruments. Moreover, the determination of Cd by those methods is time-consuming process. In contrast, the electrochemical methods have been accepted for the detection of heavy metal ions because of their excellent sensitivity, rapid analysis and low cost[18,19]. Hence, the electrochemical method has emerged as a powerful technique for the detection of heavy metal ions when compared to other methods.

In recent years, variety of porous metal oxides such as MgO[20], Co_3O_4[21] and NiO[22] were reported for the electrochemical sensors. Because, these porous metal oxides have high surface area and open porous structure which helps in the detection of heavy metal ions. The transition metal oxides with a spinel structure have attracted more interest in the wide area of research field due to their unique properties such as magnetic, electrical and optical properties[23–25]. The common chemical formula of the spinel is AB_2O_4, where A and B are the divalent and trivalent metal ions, coordinated in tetrahedral and octahedral sites, respectively[26]. Among the materials developed for the Cd detection, the spinel metal oxides are the promising materials due to high earth abundance, low cost

National Taipei University of Technology, Taipei, 106, Taiwan, Republic of China. Correspondence and requests for materials should be addressed to S.-M.C. (email: smchen78@ms15.hinet.net)

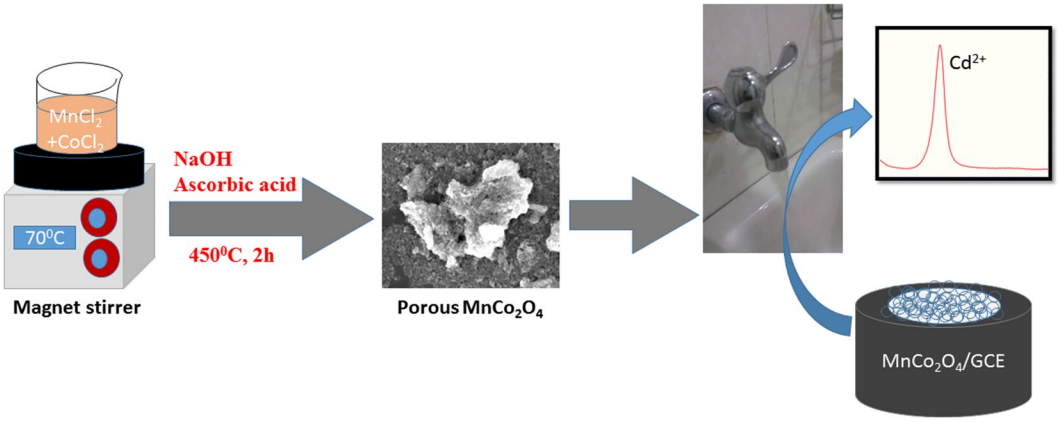

Figure 1. Preparation of porous $MnCo_2O_4$ and electrochemical detection of Cd^{2+}.

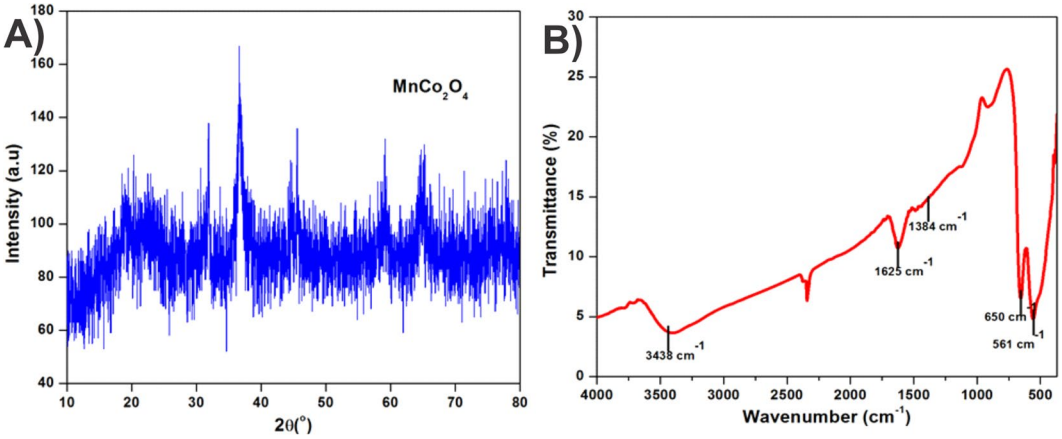

Figure 2. (**A**) XRD pattern (**B**) FTIR spectrum of porous $MnCo_2O_4$ spinel compound.

and environmentally friendly[27–29]. Hence, $MnCo_2O_4$ has been accepted as an alternative electrode material for the Cd sensor due to its excellent conductivity and tunable structural features[30,31]. $MnCo_2O_4$ lies on the normal spinel family that consists of Mn^{2+} ions in tetrahedral sites, Co^{3+} ions in the octahedral sites and O^{-2} ions tend to coordinate both positions to frame the face centred cubic structure[32]. Besides sensors, $MnCo_2O_4$ has been widely utilized in alkaline fuel cells[33], solid oxide fuel cells[34], water treatment[35] and glucose sensors[36]. In this work, we have demonstrated the synthesis of porous $MnCo_2O_4$ by simple chemical route at the low processing temperature. To the best of our knowledge, this is the first time we have reported the determination of Cd by porous $MnCo_2O_4$. Moreover, $MnCo_2O_4$ exhibited high sensitivity, excellent selectivity, wide linear concentration range and acceptable storage stability for the determination of Cd (II). The overall preparation and electrochemical pathway for the determination of Cd (II) was illustrated in Fig. 1.

Results and Discussion

Material characterizations. The crystallinity of as-prepared $MnCo_2O_4$ was confirmed by X-ray diffraction (XRD) analysis. Figure 2A depicts the XRD patterns of $MnCo_2O_4$ exhibiting the noisiest diffraction peaks which can be assigned as spinel compound. Those noises are due to the low crystallite size of the as-prepared compound. $MnCo_2O_4$ has a very noisy reflection peaks which indexed as a face centred cubic structure of $MnCo_2O_4$ with the space group fd3m (JCPDS No. 23-1237). The manganese and cobalt ions are well dispersive over octahedral and tetrahedral interstices to form the mixed valence ternary oxides as spinel $MnCo_2O_4$ crystal. The Debye-Scherrer formula (1) was used to calculate the average crystallite size of the as-prepared compound which exhibited the average crystallite size as 10 nm[37].

$$D = 0.9\lambda/(\beta \cos\theta) \quad (1)$$

λ is the X-Ray wavelength, β is the full width at the half maximum and θ is the diffraction angle.

The FT-IR spectrum is a very essential tool to investigate the functional group analysis. Figure 2B displays the FT-IR spectrum of $MnCo_2O_4$, the stretching frequency at 3405 cm^{-1} reveals the broad band adsorption peaks for adsorbed water (H-O-H)[38]. It can be clearly seen that the angular deformation of the adsorbed water molecules band appeared at 1628 cm^{-1}. The bands at 650 and 561 cm^{-1} are corresponding to the metal oxide characteristic

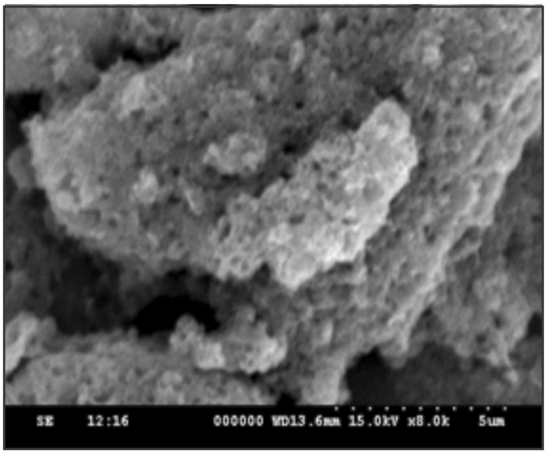

Figure 3. SEM image of porous $MnCo_2O_4$ spinel compound.

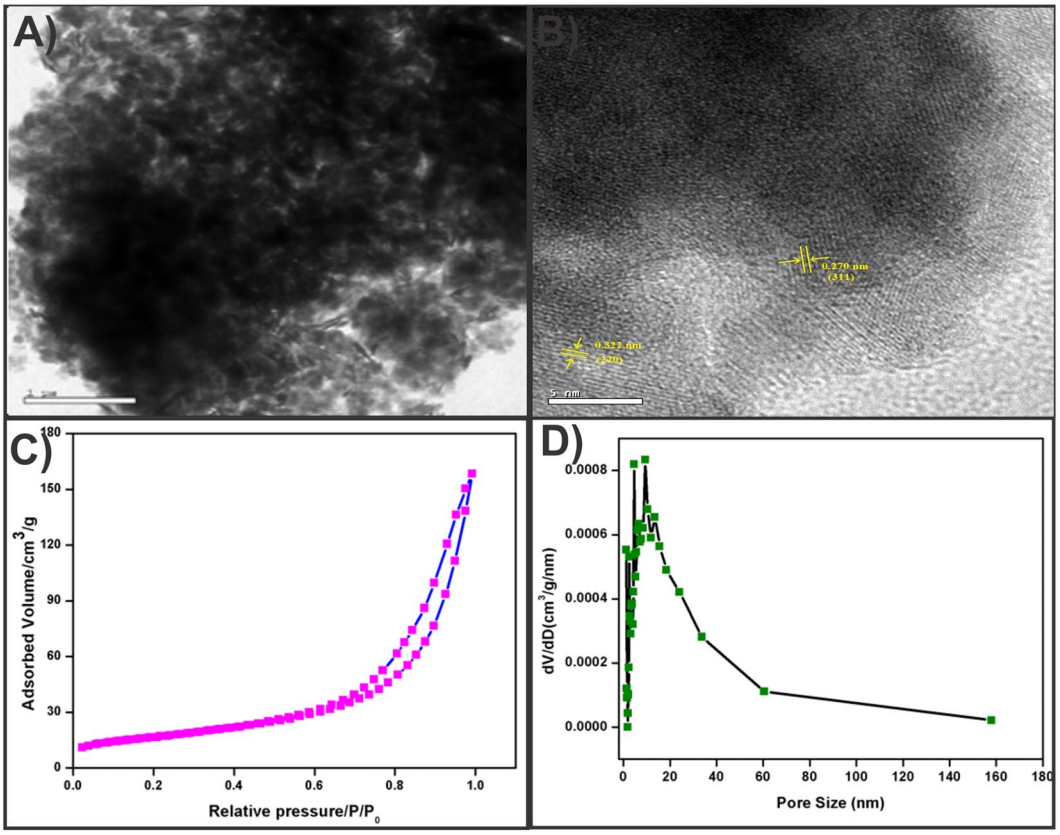

Figure 4. TEM image (**A**) and HR-TEM (**B**) of porous $MnCo_2O_4$ spinel compound (**C**) N_2 adsorption–desorption isotherms and (**D**) the pore size distribution of the $MnCo_2O_4$ spinel compound.

peaks which revealed the formation of $MnCo_2O_4$ compound[39]. The surface morphology of $MnCo_2O_4$ was investigated by SEM. The SEM images of $MnCo_2O_4$ show the flake like morphology that consists of uniform macropores (Fig. 3). Such type of the surface morphology was having a good adsorption capacity towards toxic metal ions.

The particle size and surface morphology of the porous $MnCo_2O_4$ were investigated by TEM. Figure 4A shows the TEM image of $MnCo_2O_4$ which exhibited the particles like porous morphology. The high magnification TEM image in Fig. 4B, displayed a distinct lattice fringes with an interplanar distance indexed to the crystal lattice (311) and (220) planes of spinel $MnCo_2O_4$. The specific surface area (SSA) and pore size of $MnCo_2O_4$ were examined by the N_2 adsorption-desorption isotherms. $MnCo_2O_4$ adsorption isotherms and pore size distribution (PSD) curves were shown in Fig. 4(C,D). The specific surface area ($58.82\ m^2\ g^{-1}$) was calculated by Brunauer-Emmett-Teller (BET) method for the as-prepared $MnCo_2O_4$ compound. The wide pore size distribution range (2–33 nm) was observed and also the total pore volume was calculated as $0.2454\ cm^3\ g^{-1}$ by using the BJH method.

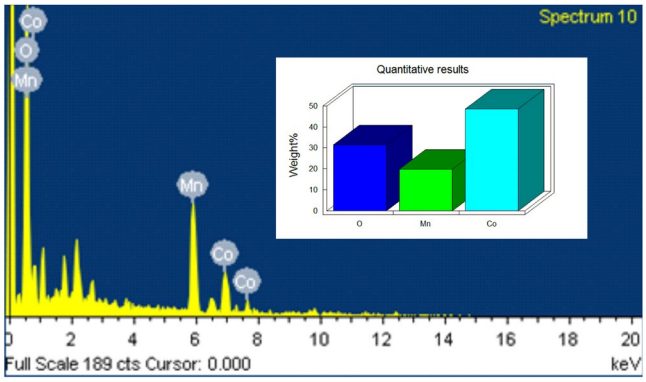

Figure 5. EDX spectrum and element weight % bar diagram of $MnCo_2O_4$.

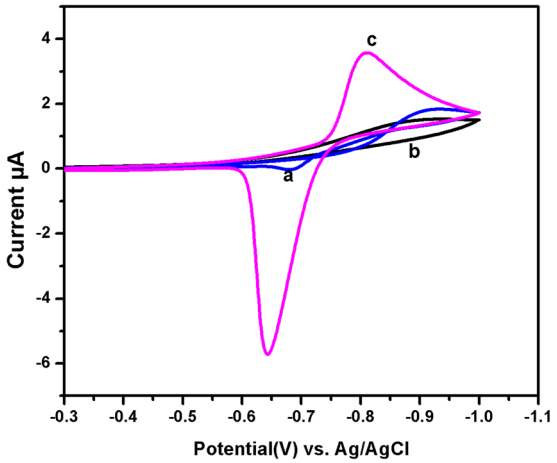

Figure 6. CV response of bare GCE in the presence of Cd (II) (a) $MnCo_2O_4$/GCE (c) and in the absence of $MnCo_2O_4$/GCE (b) in the acetate buffer (pH 5) solution containing 50 µg L^{-1} of Cd (II).

Moreover, the presence of elements in $MnCo_2O_4$ compound was confirmed by EDX analysis and shown in Fig. 5. The EDX spectrum of $MnCo_2O_4$ exhibits the signal for Mn, Co and O with the weight percentage of 11.47%, 26.12% and 65.41%, respectively. These results confirmed that the as-prepared compound was porous $MnCo_2O_4$ spinel.

Electrochemical behavior of Cd (II). CV response of $MnCo_2O_4$/GCE was tested in the presence of 50 µg L^{-1} Cd (II) at a scan rate of 50 mV s^{-1} in acetate buffer solution. Figure 6 shows the electrochemical response of bare GCE (a) which exhibited the weak redox peak for 50 µg L^{-1} of Cd (II). It can be obviously seen that there were no peaks appeared for $MnCo_2O_4$/GCE (b) in the absence of Cd (II). However, a sharp and well-defined redox peak was observed for the porous $MnCo_2O_4$/GCE (c) with higher current response when compared with bare GCE. The obtained oxidation peak current from the porous $MnCo_2O_4$ was higher than that of the bare GCE. In addition, the porous $MnCo_2O_4$ provides a highly rough surface of the electrode which has a larger surface area with more active sites for Cd (II) accumulation.

Optimization of parameters. The effect of pH (acetate buffer solution) on the electrochemical performance of our proposed electrode was examined in the range of pH 2.0–6.0. It can be seen from the Fig. 7A, the maximum peak current was appeared at pH 5.0. Therefore, the pH 5.0 acetate buffer solution was used as electrolyte for the further detection of the Cd (II). The deposition potential is an important parameter in the detection of Cd (II). Therefore, the effect of deposition potential was investigated in presence of Cd (II) at pH 5.0 solution after 200 s of accumulation in the potential range from −0.6 to −1.2 V. Figure 7B depicts electrochemical activity for deposition potential showing the maximum current reached in the deposition potential of −1.0 V. Therefore, −1.0 V was fixed as the optimum deposition potential. The effect of the deposition time on $MnCo_2O_4$/GCE current response was also investigated from 50 s to 300 s. As shown in Fig. 7C, the current response was higher for the accumulation time of 200 s. Therefore, the 200 s of deposition time was chosen for the further experiment.

The determination of $MnCo_2O_4$ was tested by the successive additions of different concentrations of Cd (II) ions (Fig. 8A). Response of $MnCo_2O_4$/GCE was recorded towards various concentrations of Cd (II) from 2.3 to 120 µg L^{-1}. The noticeable current response was appeared for the addition of 2.3 µg L^{-1} of Cd (II), further the

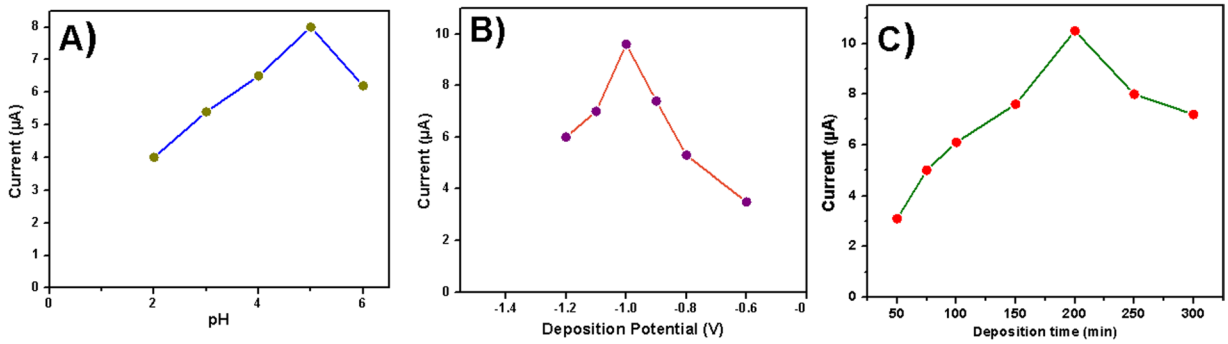

Figure 7. Effect of (**A**) pH of acetate buffer (**B**) Deposition potential of cadmium (**C**) Deposition time of cadmium on the DPSAV current in acetate buffer solution contained 50 μg L^{-1} of Cd (II) ion.

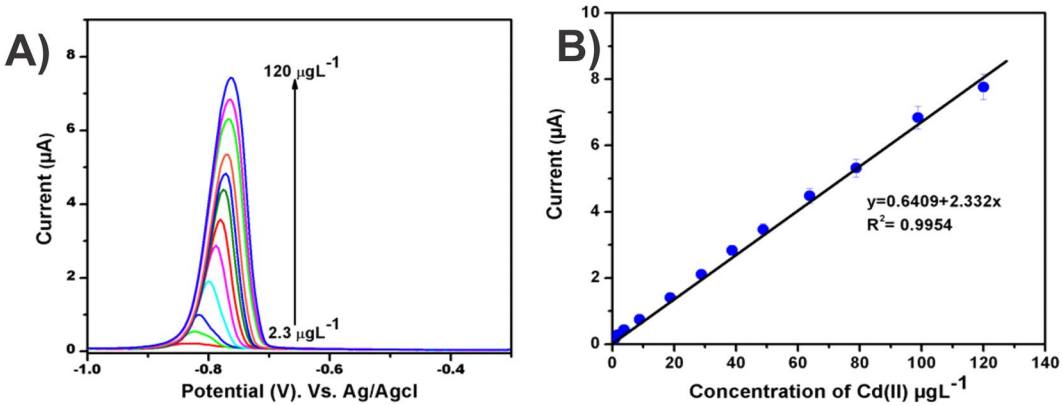

Figure 8. (**A**) Responses of $MnCo_2O_4$ modified GCE for the addition of different concentrations of Cd (II) from 2.3 to 120 μg L^{-1}. (**B**) The corresponding linear plot for I_{pa} vs. concentration of Cd (II).

Modified electrode	Method	Linear range (μg L^{-1})	LOD (μg L^{-1})	Ref.
Nafion/Bi/NMC	DPASV	2–100	1.5	40
TM-MCM-41-CPE	Potentiometric	—	435	41
SnO_2 quantum dots	CV	4990–44910	499	42
RGO/Bi	DPASV	20–120	2.8	43
G/PANI/PS-SPCE	SWASV	0–500	4.43	44
Bi/CNT	SWASV	2–100	0.7	45
2-benzothiazolethiol/amorphous silica- CPE	DPASV	—	11	46
Porous $MnCo_2O_4$/GCE	DPASV	2.3–120	0.72	Present work

Table 1. Comparison for the analytical performance of other reported methods. NMC- Nitrogen doped microporous carbon, TM-MCM- Thiomorpholine-functionalized-Mobil Composition Matter, CPE- carbon paste electrode, RGO- Reduced graphene oxide, G/PANI/PS-Graphene/polyaniline/polystyrene nanoporous fibers, CV- Cyclic Voltammetry, DPASV-Differential pulse anodic stripping voltammetry, SWASV-Square-wave anodic stripping voltammetry.

peak current was increased with increasing the concentration of Cd (II). The gradual positive shift in the stripping potentials of Cd (II) might be due to the increase in the interfacial thickness of Cd (II)-$MnCo_2O_4$. A linear concentration range was obtained from 2.3 to 120 μg L^{-1} with the correlation coefficient of $R^2 = 0.9954$ (Fig. 8B). The limit of detection was calculated as 0.72 μg L^{-1}, limit of quantification was obtained as 0.91 μg L^{-1}. The sensitivity of the proposed sensor was calculated by dividing the slope of the calibration plot by electroactive area, the calculated sensitivity is 7.7355 μA μg^{-1} L cm^{-2}. The analytical performances of the proposed sensor have been compared with previously reported other sensors (Table 1).

Interference study. In order to evaluate the selectivity of the fabricated sensor, it was investigated in the presence of various potentially interfering ions. Figure 9 shows the current responses for (50 μg L^{-1}) Cd (II) in the presence of a 3-fold excess concentration of metal ions such as Cu^{2+}, Pb^{2+} and Hg^{2+}. The results showed that the interference signal was less than 1% for interfering ions. Therefore, the proposed sensor material selectively

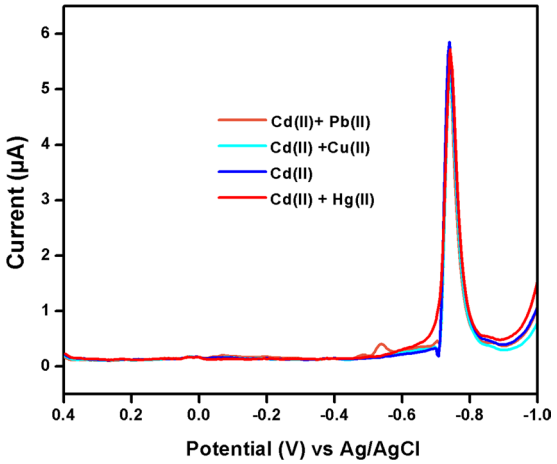

Figure 9. Effect of interference species on the detection of cadmium at $MnCo_2O_4$. Peak current response of 50 μg L^{-1} Cd (II) in the presence of 3-fold of Cu^{2+}, Pb^{2+} and Hg^{2+}.

Sample	added (μM)	Found (μM)	Recovery (%)
1	3.0	2.85	95.00
2	15	15.02	100.13
3	50	49.95	99.90
4	100	98.89	98.89

Table 2. Determination of Cd (II) in water samples by $MnCo_2O_4$ modified GCE.

detected Cd (II) in the presence of interferents. These studies resulted that $MnCo_2O_4$ exhibited good selectivity for the detection of Cd (II) in the presence of other interference. Therefore, the proposed sensor material is suitable for the practical applications.

Real sample analysis. In order to evaluate the reliability of proposed sensor, the determination of Cd (II) was examined in water samples. An optimized experimental condition was applied for the detection of Cd (II) in tap water. The standard addition method was used to detect Cd (II) and the calculated recovery results were presented in Table 2. It can be seen that the average recoveries of Cd (II) were 95.33–100.3% in tap water samples. These results evinced that the practicability of the proposed sensor towards the determination of Cd (II) in water samples.

Stability, repeatability and reproducibility. The five different sensing electrodes were prepared under the same experimental conditions followed from section (Electrochemical behavior of Cd (II)) and observed the efficiency of the Cd (II) detection. The fabricated sensors showed almost same response for all the electrodes and revealed reproducibility with the RSD of 3.80% for the determination of Cd (II). These sensor electrodes were stored at room temperature over 30 days. After that it was retained about 90% of its initial response which confirmed that $MnCo_2O_4$ modified electrode has good storage stability. In addition, the sensor also has a good repeatability with RSD value of 3.2%, for the five repeated successive measurements of single modified electrode. These results disclose the proposed sensor material has excellent stability repeatability and reproducibility which endorsed that $MnCo_2O_4$/GCE is suitable for the practical applications.

Conclusions

In summary, the honeycomb-like porous $MnCo_2O_4$ spinel was prepared from the simple facile method and subsequent calcination. The simple electrochemical technique was applied to detect the Cd ion by DPASV based on porous $MnCo_2O_4$ modified electrode. The developed sensor shows a wide linear concentration range from 2.3 to 120 μg L^{-1}, lowest detection limit of 0.72 μg L^{-1} and excellent sensitivity of 7.7355 μA μg^{-1} L cm^{-2}. The analytical performances of the developed sensor were comparable with the previous results. Moreover, $MnCo_2O_4$/GCE exhibits good storage stability, acceptable selectivity, excellent repeatability and reproducibility. In addition, the developed $MnCo_2O_4$/GCE validates the practicability towards the determination of Cd (II) in water samples.

Experimental

Chemicals and apparatus. Manganese chloride, cobalt chloride, cadmium nitrate, sodium hydroxide and ascorbic acid were obtained from Sigma–Aldrich. The supporting electrolyte of acetate buffer (pH 5) solution was prepared by using 0.05 M sodium acetate and glacial acetic acid. All the chemicals used were of analytical grade and used as received without purification. Cyclic voltammetry (CV) and differential pulse anodic stripping voltammetry (DPASV) measurements were performed by the CHI 900 electrochemical workstations. Scanning

electron microscopy (SEM) was performed using Hitachi S-3000 H electron microscope, Fourier transform infrared spectroscopy (FT-IR) was carried out by using JASCO FT/IR-6600 instrument. The conventional three-electrode system was used for the electrochemical experiments, the modified glassy carbon electrode (GCE) was used as a working electrode (electrode area: 0.07 cm^2), saturated Ag/AgCl used as a reference electrode and platinum electrode used as the auxiliary electrode.

Synthesis of porous $MnCo_2O_4$ spinel oxide. For the preparation of porous $MnCo_2O_4$ composite, the molar ratio (1:2) of $MnCl_2$ and $CoCl_2.6H_2O$ were dissolved in 50 ml distilled water and stirred for 30 minutes. Then, 0.2 M NaOH was added drop-wise with constant stirring and after that 0.1 M ascorbic acid was slowly added to the suspension. Suspension temperature was maintained at 60–70° C for 1 hr. Finally, the precipitate was filtered and washed with ethanol and distilled water. The precipitate was dried at room temperature. After that the dried samples were calcined in a hot air oven at 450° C for 2 hr. Finally, the black color porous $MnCo_2O_4$ was obtained.

Fabrication of electrode and operating condition. Glassy carbon electrode was precleaned with alumina powder and sonicated about 2 mins in ethanol and double distilled water. The adsorbed alumina slurry on the surface of GCE was removed by washing with double distilled water and dried in hot air oven. As-prepared composite was re-dispersed in water and sonicated to get well uniform suspension. A mirror cleaned GCE was fabricated with the suspension of $MnCo_2O_4$ by drop cast (6 µL) method and dried in a hot air oven at 35° C for 10 min. The fabricated $MnCo_2O_4$/GCE was further used for the electrochemical measurements.

All the experimental conditions were optimized by voltammograms. The electrochemical cell contains 10 mL of desired pH of acetate buffer (0.05 M) solution. The differential pulse Anodic stripping voltammograms were recorded from −0.3 to 1.1 V, applied potential of preconcentration of Cd (II) was −1.0 V and 200 s of preconcentration time. The calibration curve was obtained by plotting the peak current against deposition of cadmium potential range and deposition of cadmium accumulation time. The electrode was polished after each measurement with a clean paper.

References

1. Keawkim, K., Chuanuwantanakul, S., Chailapakul, O. & Motomizu, S. Determination of lead and cadmium in rice samples by sequential injection/anodic stripping voltammetry using a bismuth film/crown ether/Nafion modified screen-printed carbon electrode. *Food contr.* **31**, 14–21 (2013).
2. Vieria, R. S., Oliveira, M. L. M., Guibal, E., Rodrequez- Castellon, E. & Beppu, M. M. Copper, mercury and chromium adsorption on natural and crosslinked chitosan films: An XPS investigation of mechanism. *Colloids surf. A.* **374**, 108–114 (2011).
3. Gupta, V. K., Ali, I. & Aboul-Enein, H. Y. Metal Ions Speciation in the Environment: Distribution, Toxicities and Analyses. *Dev. Environ. Sci.* **5**, 33–56 (2007).
4. Ikeda, M., Watanabe, T., Ohashi, F. & Shimbo, S. Effects of variations in cadmium and lead levels in river sediments on local foods and body burden of local residents in non-polluted areas in Japan. *Biol. TraceElem. Res.* **133**, 255–264 (2010).
5. Gonzalez-Estecha, M. *et al*. Blood lead and cadmium levels in a six hospital employee population. *PESA study, 2009, J. Trace Elem. Med. Biol.* **25**, 22–29 (2011).
6. Chang, I. C., Hsiao, T.-Y., Yu, Y.-H. & Ma, H.-W. Identification of pollution source of Cadmium in soil. *Environ. Sci. Pollut. Res.* **14**, 49–59 (2005).
7. Prange, A. Characterization of the cytosolic distribution of priority pollutant metals and metalloids in the digestive gland cytosol of marine mussels: seasonal and spatial variability. *Sci. TotalEnviron.* **470**, 1159–170 (2014).
8. Ruttens, A., Smeets, K., Clijsters, H. & Vangronsveld, J. Cadmium exposure in the population: from health risks to strategies of prevention. *Biometals.* **23**, 769–782 (2010).
9. Iqbal, J., Shah, M. H. & Akhter, G. Characterization, source apportionment and health risk assessment of trace metals in freshwater Rawal Lake, Pakistan. *J. Geochem. Explor.* **125**, 94–101 (2013).
10. Australian Water Drinking Guidelines, Inorganic Chemicals: Cadmium, Fact Sheet No. 44, NHMRC and Agriculture and Resource Management Council of Australia and New Zealand (1996).
11. Guidelines for Drinking Water Quality, World Health Organization, Geneva, 4th edn (2011).
12. Thompson, R. Q. & Christopher, S. J. Novel separation for the determination of cadmium by isotope dilution ICP-MS in samples containing high concentrations of molybdenum and tin. *Anal. Methods.* **5**, 1346–1351 (2013).
13. Murphy, K. E. & Vetter, T. W. Recognizing and overcoming analytical error in the use of ICP-MS for the determination of cadmium in breakfast cereal and dietary supplements. *Anal. Bioanal. Chem.* **405**, 4579–4588 (2013).
14. Matsumoto, A. *et al*. Determination of cadmium by an improved double chamber electrothermal vaporization inductively coupled plasma atomic emission spectrometry. *Microchem. J.* **95**, 85–89 (2010).
15. Parham, H., Pourreza, N. & Rahbar, N. Solid phase extraction of lead and cadmium using solid sulfurase new metal extract or prior to determination by flame atomic absorption spectrometry. *J. Hazard. Mater.* **163**, 588–592 (2009).
16. Wan, Z., Xu, Z. & Wang, J. Flow injection on-line solid phase extraction for ultra- trace lead screening with hydride generation atomic fluorescence spectrometry. *Analyst.* **131**, 141–147 (2006).
17. Hu, Q. F., Yang, G. Y., Zhao, Y. Y. & Yin, J. Y. Determination of copper nickel, cobalt, silver, lead, cadmium, and mercury ions in water by solid-phase extraction and the RP-HPLC with UV–vis detection. *Anal. Bioanal. Chem.* **375**, 831–835 (2003).
18. Turyan, I. & Mandler, D. Electrochemical mercury detection. *Nature* **362**, 703–704 (1993).
19. Dai, X., Nekrassova, O., Hyde, M. E. & Compton, R. G. Anodic stripping voltammetry of arsenic (III) using gold nanoparticle-modified electrodes. *Analytical chemistry* **76**, 5924–5929 (2004).
20. Wei, Y., Yang, R., Yu, X. Y., Wang, L., Liu, J. H. & Huang, X. J. Stripping voltammetry study of ultra-trace toxic metal ions on highly selectively adsorptive porous magnesium oxide nano flowers. *Analyst.* **137**, 2183–2191 (2012).
21. Liu, Z. G., Chen, X., Liu, J. H. & Huang, X. J. Well-arranged porous Co_3O_4 microsheets for electrochemistry of Pb(II) revealed by stripping voltammetry. *Electrochemistry Communications* **30**, 59–62 (2013).
22. Wu, Z., Jiang, L., Zhu, Y., Xu, C., Ye, Y. & Wang, X. Synthesis of mesoporous NiO nanosheet and its application on mercury (II) sensor. *Journal of Solid State Electrochemistry* **16**, 3171–3177 (2012).
23. Liang, Y. Y. *et al*. covalent hybrid of spinel manganese-cobalt oxide and graphene as advanced oxygen reduction electrocatalysts. *J. Am. Chem. Soc.* **134**, 3517–3523 (2012).
24. Bragg, W. H. The structure of magnetite and the spinels. *Nature* **95**, 561 (1915).

25. Choi, H. C., Shim, J. H. & Min, B. I. Electronic structures and magnetic properties of spinel $ZnMn_2O_4$ under high pressure. *Phys. Rev. B.* **74**, 172103–172106 (2006).
26. Cheng, F. Y. *et al.* Rapid room-temperature synthesis of nanocrystalline spinels as oxygen reduction and evolution electrocatalysts. *Nat. Chem.* **3**, 79–84 (2011).
27. Naik, K. K. *et al.* Enhanced electron field emission from $NiCo_2O_4$ nanosheet arrays. *Mater. Res. Express.* **2**, 95011 (2015).
28. Li, L. *et al.* One-dimension $MnCo_2O_4$ nanowire arrays for electrochemical energy storage. *Electrochim. Acta.* **116**, 467–474 (2014).
29. Gomez, J. & Kalu, E. E. High-performance binder-free Co–Mn composite oxide supercapacitor electrode. *J. Power Sources* **230**, 218–224 (2013).
30. Zhang, Y. *et al.* Z. Electrospun graphene decorated $MnCo_2O_4$ composite nanofibers for glucose biosensing. *Biosens. Bioelectron.* **66**, 308–315 (2015).
31. Ge, X. *et al.* Dual-phase spinel $MnCo_2O_4$ and spinel $MnCo_2O_4$/nanocarbon hybrids for electrocatalytic oxygen reduction and evolution. *ACS Appl. Mater. Interfaces* **6**, 12684–12691 (2014).
32. Schreyeck, L., Wlosik, A. & Fuzellier, H. Influence of the synthesis route on $MgAl_2O_4$ spinel properties. *J. Mater. Chem.* **11**, 483–486 (2001).
33. Nissinen, T., Valo, T., Gasik, M., Rantanen, J. & Lampinen, M. Microwave Synthesis of Catalyst Spinel $MnCo_2O_4$ for Alkaline Fuel Cell. *J. Power Sources* **106**, 109–115 (2002).
34. Liu, H. Y. *et al.* Electrochemical Performances of Spinel Oxides as Cathodes for Intermediate Temperature Solid Oxide Fuel Cells. *Int. J. Hydrogen Energy* **38**, 1052–1057 (2013).
35. Yang, W. S., Hao, J. H., Zhang, Z., Lu, B. P., Zhang, B. L. & Tang, J. L. Synthesis of Hierarchical MnCo2O4.5 Nanostructure Modified MnOOH Nanorods for Catalytic Degradation of Methylene Blue. *Catal. Commun.* **46**, 174–178 (2014).
36. Zhang, Y. Y. *et al.* Synthesis of $MnCo_2O_4$ Nanofibers by Electrospinning and Calcination: Application for a Highly Sensitive Non-Enzymatic Glucose Sensor. *J. Mater. Chem. B.* **2**, 529–535 (2014).
37. Tholkappiyan, R. & Vishista, K. Influence of lanthanum on the optomagnetic properties of zinc ferrite prepared by combustion method. *Physica B.* **448**, 177–183 (2014).
38. Subramanian, V., Hall, S. C., Smith, P. H. & Rambabu, B. Mesoporous anhydrous RuO2 as a supercapacitor electrode material. *Solid State Ionics* **175**, 511–515 (2004).
39. Rojas, R. M., Vila, E., Garcı´a, O. & de Vidales, J. L. M. Thermal behaviour and reactivity of manganese cobaltites $Mn_xCo_{3-x}O_4$ ($0.0 \leq x \leq 1.0$) obtained at low temperature. *J Mater Chem.* **4**, 1635–1639 (1994).
40. Xiao, L. *et al.* Simultaneous detection of Cd (II) and Pb (II) by differential pulse anodic stripping voltammetry at a nitrogen-doped microporous carbon/nafion/bismuth-film electrode. *Electrochim. Acta* **143**, 143–151 (2014).
41. Ganjali, M. R. *et al.* Thiomorpholine- functionalized nanoporous mesopore as a sensing material for Cd^{2+} carbon paste electrode. *J. Solid State Electr.* **14**, 1359–1366 (2010).
42. Bhanjana, G., Dilbaghi, N., Kumar, R., Umar, A. & Kumar, S. SnO_2 quantum dots as novel platform for electrochemical sensing of cadmium. *Electrochim. Acta* **169**, 97–102 (2015).
43. Sahoo, P. K., Panigrahy, B., Sahoo, S., Satpati, A. K., Li, D. & Bahadur, D. Insitu synthesis and properties of reduced graphene oxide/Bi nanocomposites: as an electro active material for analysis of heavy metals. *Biosens. Bioelectron.* **43**, 293–296 (2013).
44. Promphet, N., Rattanarat, P., Rangkupan, R., Chailapakul, O. & Rodthongkum, N. An electrochemical sensor based on graphene/polyaniline/polystyrene nanoporous fibers modified electrode for simultaneous determination of lead and cadmium, *Sens. Actuators B Chem.* **207**, 526–534 (2015).
45. Hwang, G. H., Han, W. K., Park, J. S. & Kang, S. G. Determination of trace metals by anodic stripping voltammetry using a bismuth-modified carbon nanotube electrode. *Talanta* **76**, 301–308 (2008).
46. Marino, G., Bergamini, M. F., Teixeira, M. F. S. & Cavalheiro, E. T. G. Evaluation of a carbon paste electrode modified with organo functionalized amorphous silica in the cadmium determination in a differential pulse anodic stripping voltammetric procedure. *Talanta* **59**, 1021–1028 (2003).

Acknowledgements

This project was supported by the National Science Council and the Ministry of Education of Taiwan (Republic of China).

Author Contributions

M.V. prepared the composites and material characterizations. M.V. had written the manuscript and S.M.C. supervised and finalized the project.

Additional Information

Competing Interests: The authors declare that they have no competing interests.

Publisher's note: Springer Nature remains neutral with regard to jurisdictional claims in published maps and institutional affiliations.